α-glucosyl-rutin activates immediate early genes in human induced pluripotent stem cells

Tomoko Miyake [a,*], Munekazu Kuge [a], Yoshihisa Matsumoto [b], Mikio Shimada [b,*]

[a] Cosmetic R&D Department, Takara Belmont Corp, 7-1-19 Akasaka, Minato-ku, Tokyo 107-0052, Japan
[b] Laboratory for Zero-Carbon Energy, Institute of Innovative Research, Tokyo Institute of Technology, 2-12-1 Ookayama, Meguro-ku, Tokyo 152-8550, Japan

ARTICLE INFO

ABSTRACT

Rutin is a natural flavonoid glycoside found in several vegetables and fruits such as buckwheat and onion. Rutin has a range of pharmacological effects that include anti-oxidant, anti-inflammation, anti-bacterial, and anti-cancer activities. α-glucosyl-rutin (AGR) is a derivative of rutin with increased water solubility that is used in cosmetics and foods. However, the effects of AGR on cellular responses have not been clarified, especially in stem cells. Induced pluripotent stem cells (iPSCs) show high proliferative activity and pluripotency; however, regulation of molecular machinery such as cell cycle, metabolism, and DNA repair differs between iPSCs and somatic cells. Here, we compared the effects of AGR on iPSCs and differentiated cells (fibroblasts and skin keratinocytes). AGR-treated iPSCs exhibited increased cell viability. RNA sequencing and reverse transcriptase PCR analysis revealed that AGR induced expression of immediate early genes (IEGs) and differentiation-related genes in iPSCs. Our results suggest that AGR may activate differentiation signals mediated by IEG responses in iPSCs, resulting in altered metabolic activity and increased cell viability.

1. Introduction

Pluripotent stem cells (PSCs), such as embryonic stem cells and induced pluripotent stem cells (iPSCs) are defined as high proliferative cells with a short G1 phase that have specifically regulated molecular machinery, e.g., cell cycle, metabolism, and DNA repair (Liu et al., 2019; Tsogtbaatar et al., 2020; Vitale et al., 2017; Zhang et al., 2018). In previous reports, we analyzed the DNA damage response in human iPSCs and differentiated cells derived from iPSCs (neural stem/precursor cells and skin keratinocytes [KCs]) (Miyake et al., 2019; Shimada et al., 2019); these studies demonstrated that iPSCs were highly proliferative with increased DNA damage response and apoptosis in comparison with the behavior of differentiated cells, suggesting specific gene regulation in iPSCs.

Rutin is a flavonoid glycoside that is found in several vegetables and fruits such as buckwheat and onion. Rutin has known pharmacological effects, including anti-oxidant, anti-diabetic, anti-inflammation, anti-bacterial, and anti-cancer activities (Ganeshpurkar et al. 2017; Prasad et al., 2019). α-glucosyl-rutin (AGR) was developed by enzymatic glycosylation to improve the water solubility of rutin, and AGR has been used as an antioxidant and colorant for cosmetics and foods in Japan (Engen et al., 2015; Shimoi et al., 2003; Suzuki et al., 1991). Radio-protective effects of flavonoids including AGR have been reported (Aizawa et al., 2018). However, the effects of AGR on cellular response remain unclear, especially in stem cells.

Cellular homeostasis is maintained by regulating gene expression in response to various stimuli. The transcription factor activator protein-1 (AP-1) is induced by stimuli such as growth factors, cytokines, bacterial infections, and genotoxic and chemical stress (Bejjani et al., 2019; Shaulian et al., 2002). AP-1 is dimeric complex composed of proteins from the JUN, FOS, and ATF families and regulates cellular responses including cell proliferation, differentiation, and survival. *JUN* and *FOS* genes are also known as major immediate early genes (IEGs). Extracellular stimulation induces IEGs such as AP-1, although these are rapidly activated within minutes and often have a transient response (Bahrami et al., 2016). IEG responses play an important role in cell cycle regulation and are involved in cellular responses such as cell proliferation and differentiation, and more than 100 IEGs, including *JUN*, *FOS*, *ATF3*, and *EGR1*, have so far been reported (Arner et al., 2015; Murai et al., 2020). The IEG response differs depending on the cell type and stimuli.

Extracellular stimuli activate intracellular mitogen-activated protein kinase (MAPK) pathways such as extracellular signal-regulated kinase, and then the MAPK cascade activates transcription factors (Bahrami et al., 2016). Serum response factor (SRF) is a major regulator of IEGs and involved in various cellular responses including proliferation, adhesion, and differentiation (Gualdrini et al., 2016; Weinhold et al., 2000). SRF increase *FOS* and *EGR1* expression, then JUN and FOS promote cell cycle by upregulating expression of *CCND1* (gene product: cyclin D1) (Bahrami et al., 2016; Langfermann et al., 2018; Shaulian et al., 2002).

In this study, we compared AGR-induced cellular responses including cell viability, cell death, cell cycle, reactive oxygen species (ROS) generation, and metabolism among genetically identical cells, fibroblasts, iPSCs, and iPSC-derived KCs. We performed comprehensive gene expression analysis using RNA-seq and demonstrated that AGR activates the IEG response. Furthermore, we found transient increasing of cellular metabolic products, acetyl-CoA (Ac-CoA), lactate, and glucose in AGR treated iPSCs. These results suggest that AGR transiently induce IEG response and cellular metabolic change in iPSCs.

2. Materials and methods

2.1. Cell culture

Primary human skin fibroblasts (NB1RGB) and human iPSCs (201B7) were obtained from Riken Cell Bank. *C*2 iPSCs have been previously generated from NB1RGB (Shimada et al., 2019). NB1RGB and human colon cancer cells (HCT116) were cultured in Dulbecco's modified Eagle's medium (Sigma-Aldrich, USA) containing 10% fetal bovine serum (Hyclone, GE Healthcare, USA), 100 U/mL penicillin, and 100 μg/mL streptomycin. iPSCs were cultured in feeder-free conditions. *C*2 iPSCs and 201B7 cells were maintained in Nutristem XF/FF Culture Medium (Stemgent, USA) on iMatrix 511 (Nippi, Japan)-precoated dishes at 37 °C in 5% CO_2 incubator. Cell passage was performed with TrypLE Select (Thermo Fisher Scientific, USA). Following passage, cells were cultured for 24 h in Nutristem XF/FF Culture Medium supplemented with 5 μM Rho-associated protein kinase inhibitor (Y27632) (WAKO, Japan).

2.2. Differentiation of iPSCs into keratinocytes

*P*1 KCs were differentiated from *C*2 iPSCs as previously described (Miyake et al., 2019). Briefly, on day 0, *C*2 iPSCs were cultured in Nutristem XF/FF Culture Medium supplemented with 5 μM Y27632 on iMatrix 511. On day 1, culture medium was replaced with defined keratinocyte serum-free medium (DKSFM) supplemented with 1 μM retinoic acid (Sigma-Aldrich) and 10 ng/mL bone morphogenic protein 4 (R&D Systems, USA). On day 4, culture medium was replaced with DKSFM supplemented with 20 ng/mL epidermal growth factor (EGF) (R&D Systems). On day 14, the first passage was performed. First passage cells were cultured in DKSFM supplemented with 20 ng/mL EGF and 10 μM Y27632 for 1 week on dishes precoated with 0.03 mg/mL type I collagen (Advanced BioMatrix, USA) and 0.01 mg/mL fibronectin (Sigma-Aldrich); these cells were then used as *P*1 KCs.

2.3. WST-8 assay

*C*2 iPSCs, *P*1 KCs, and NB1RGB fibroblasts, 201B7, and HCT116 cells at 5×10^3 / well were cultured in a 96-well plate. NB1RGB fibroblasts and HCT116 cells were cultured for 1 day, *C*2 iPSCs and 201B7 cells for 2 days, and *P*1 KCs for 1 week. Cells were then treated with AGR (Toyo Sugar Corp., Japan) at 0.05–100 μM for 24 h; cell viability was then analyzed using a Cell Counting Kit-8 (Dojindo, Japan). Cells were incubated for 2 h with medium containing assay reagents in a 96 well plate, and then absorbance was measured at 450 nm with an iMark ™ Microplate Absorbance Reader (Bio Rad, USA).

2.4. Cell number measurement

NB1RGB fibroblasts, *C*2 iPSCs, and *P*1 KCs were cultured in a 24-well plate. The initial cell number was 3×10^4 / well, 2×10^4 / well, and 4×10^4 / well, respectively. NB1RGB fibroblasts were cultured for 1 day, *C*2 iPSCs for 2 days, and *P*1 KCs for 1 week. Cells were then treated with AGR at 0.05–100 μM for 24 h. Next, cells were collected from a 24-well plate and the cell number was then analyzed using a Coulter counter Z1 (Beckman Coulter, USA).

2.5. Cell cycle analysis

After treating NB1RGB fibroblasts, *C*2 iPSCs, and *P*1 KCs with 50 μM AGR for 24 h, cells at 80–90% confluency on 6-cm dish were harvested. The cells were fixed overnight with 100% methanol at −80 °C, and then washed with 0.1% bovine serum albumin (BSA)/PBS. The cells were stained with 10 μg/mL Propidium Iodide (PI)/PBS containing 100 μg/mL RNase A and 0.02% sodium azide for 1 h at room temperature in the dark. The cell cycle was analyzed using flow cytometry Cell Lab Quanta SC (Beckman Coulter).

2.6. TUNEL assay

2×10^4 cells / well of NB1RGB fibroblasts, *C*2 iPSCs, and *P*1 KCs were cultured on an 8-well plate. NB1RGB fibroblasts were cultured for 1 day, *C*2 iPSCs for 2 days, and *P*1 KCs for 1 week. Cells were then treated with 50 μM AGR for 24 h. Apoptotic cells were detected by TUNEL assay using the Apoptag Fluorescent Direct in situ Apoptosis Detection Kit (Merck Millipore, USA), following the manufacturer's procedure. Briefly, after fixing with 100% methanol at −30° C for 10 min, ethanol: acetic acid 2: 1 was treated at −30 °C for 5 min, and the TdT enzyme was reacted at 37 °C for 1 h. The positive cell ratio in 200 or more cells was calculated by observing with a fluorescence microscope (Carl Zeiss, Germany).

2.7. Immunofluorescence

2×10^3 cells / well of *C*2 iPSCs were cultured on an 8-well plate. *C*2 iPSCs were treated with 50 μM AGR for 24 h or 1 week. The medium was changed once every few days for each medium. After PBS washing, cells were fixed with 4% paraformaldehyde at room temperature for 10 min and permeabilized with 0.5% Triton-X100/PBS at 4 °C for 5 min. Primary antibodies for OCT4 (rabbit, 1:1000, cat# 09_0023, Stemgent) and SSEA4 (mouse, 1:500, cat# sc-21704, Santa Cruz Biotechnology, USA) were diluted with 1% BSA/PBS-T, followed by incubation at room temperature for 4 h. Subsequently, after PBS-T washing, the secondary antibodies; Alexa Fluor Plus 488 (mouse, 1:2000, cat# A32723, Thermo Fisher Scientific) and Alexa Fluor Plus 594 (rabbit, 1:2000, cat# A32740, Thermo Fisher Scientific) diluted with 1% BSA/PBS-T were incubated at room temperature for 1 h. After that, cells were observed with a fluorescence microscope.

2.8. ROS measurement

1×10^4 cells / well of NB1RGB fibroblasts and *C*2 iPSCs were cultured on an 8-well plate for 3 days. 2×10^4 cells / well of *P*1 KCs were cultured for 1 week. And then cells were treated with 50 μM AGR for 24 h. ROS assay was performed using the DCFDA / H2DCFDA – Cellular ROS Assay kit (ab113851, Abcam, UK) followed by the manufacturer's procedure. Briefly, cells were stained with 20 μM DCFDA for 45 min at 37 °C in the dark. Fluorescence of the live cell was observed with a fluorescence microscope. Fluorescence intensity of each image was quantified using ImageJ.

2.9. RNA-seq

After treating NB1RGB fibroblasts, *C*2 iPSCs, and *P*1 KCs with 50 μM AGR for 4 h, total RNA was extracted using FastGene RNA premium kit (Nippon Genetics, Japan). RNA sequencing was performed in duplicate by Macrogen Japan Corp using NovaSeq6000. FASTQ files were imported into illumina BaseSpace Sequence Hub, and trimming and quality checking performed with FASTQ Toolkit and FAST QC. Differential expression analysis by DESeq2 was performed using RNA-Seq Differential Expression. Cutoff value of upregulation was log$_2$Foldchange > 1, P value < 0.01, whereas that for downregulation was log$_2$Foldchange <

− 1, P value < 0.01. Gene ontology (GO) of upregulated genes was analyzed by STRING version 11.0 (Nihashi et al., 2019; Szklarczyk et al., 2017).

2.10. RT-PCR

After treating *C*2 iPSCs, *P*1 KCs, and NB1RGB and 201B7 cells with 50 μM AGR for 0.5–24 h, total RNA was extracted using the FastGeneTM RNA Basic kit (Nippon Genetics). cDNA was synthesized with the PrimeScript ™ 1st strand cDNA Synthesis Kit (Takara Bio, Japan) from 1500 ng of total RNA, and PCR was performed with TaKaRa PCR
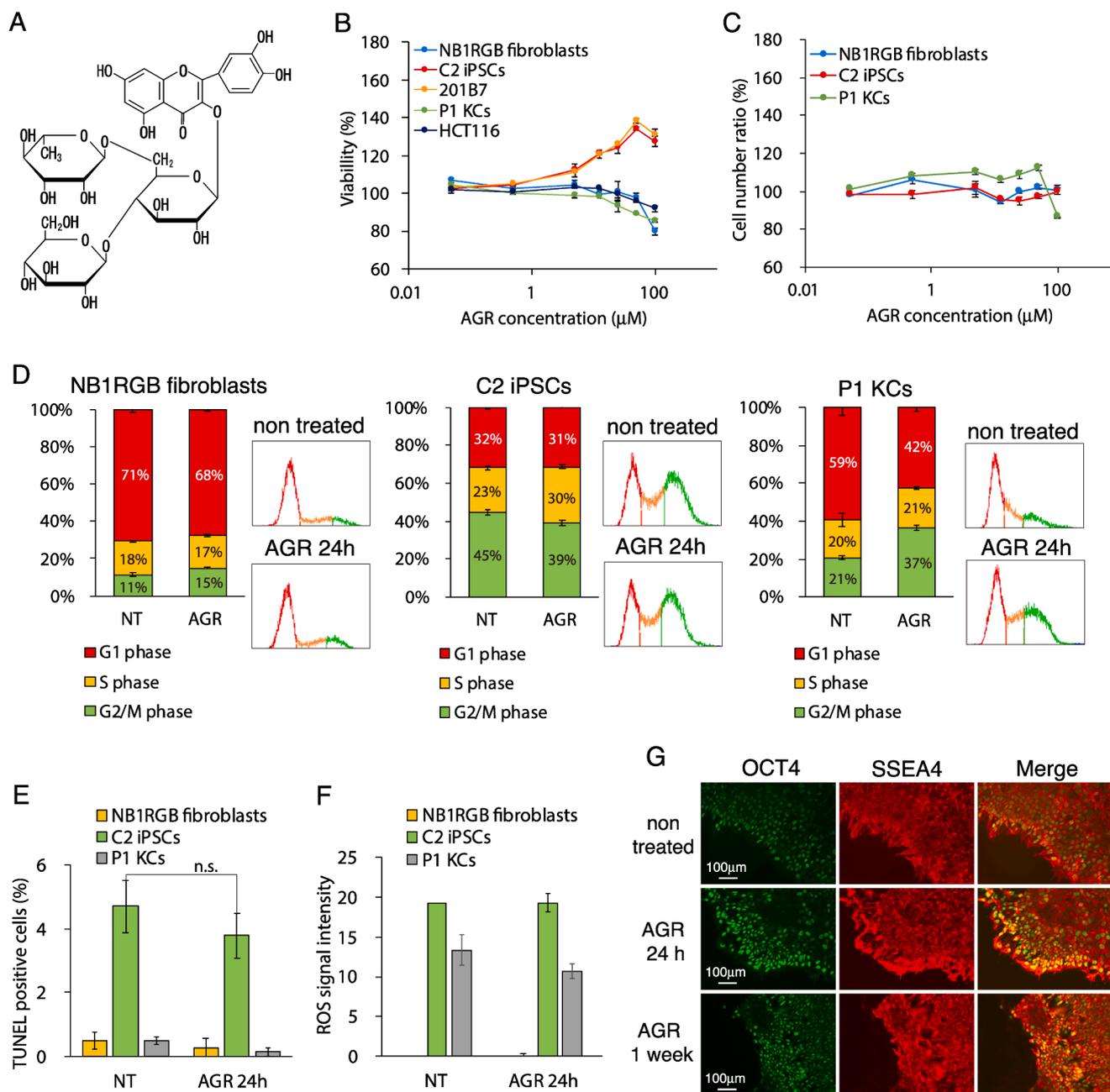

Fig. 1. α-glucosyl-rutin enhances cell viability in iPSCs. (A) Chemical structure of α-glucosyl-rutin (AGR). (B) Cell viability was measured by WST-8 assay in *C*2 iPSCs, *P*1 KCs, and 201B7, HCT116, and NB1RGB cells. Cells were treated with AGR at indicated concentrations for 24 h. Cell viability of AGR-treated cells was normalized by that of cells without treatment. (C) Cell number was measured after AGR treatment at indicated dose for 24 h in NB1RGB fibroblasts, *C*2 iPSCs, and *P*1 KCs. Cell number of AGR treated cells was normalized with no treated cells and shown as ratio. (D) Cell cycle of NB1RGB fibroblasts, *C*2 iPSCs, and *P*1 KCs and *C*2 *P*1 with 50 μM AGR for 24 h was measured. (E) TUNEL assay of NB1RGB fibroblasts, *C*2 iPSCs, and *P*1 KCs with 50 μM AGR for 24 h was performed. "n.s." indicates no significance. (F) ROS assay of NB1RGB fibroblasts, *C*2 iPSCs, and *P*1 KCs with 50 μM AGR for 24 h was performed. All experiments were independently performed three times. Error bar represented standard error. (G) Expression of pluripotency markers OCT4 and SSEA4 was compared at 50 μM AGR for 1 week and 24 h.

Thermal Cycler Dice TP 650 (Takara Bio), following the manufacturer's recommendations. cDNA was amplified by PCR using GoTaq® Green Master Mix (Promega, USA) for 30 cycles of 98 °C for 10 s, 55 °C for 5 s, and 72 °C for 1 min. Primers are shown in Supplemental Table 1. PCR products were electrophoresed and band intensity was quantified using ImageJ.

2.11. Real time PCR (qRT-PCR)

For qRT-PCR, the cDNA and primers described in RT-PCR were used. qRT-PCR was performed using TB Green Premix Ex Taq II (Takara Bio) and EcoTM RealTimePCR System (Illumina, USA) under the manufacturer's recommended conditions. First, Taq polymerase was activated at 95 °C for 30 s. Thereafter, PCR was performed for 40 cycles of 95 °C for 5 s and 60 °C for 1 min. Each standard were prepared using cDNA diluted in six steps. The correlation coefficient of each standard was 0.99 or more. The expression level in each sample was calculated from the standard and corrected by GAPDH. Primer sets are shown in Supplemental Table 1.

2.12. Cellular metabolism assay

4.5×10^5 cells of *C*2 iPSCs and 6.5×10^5 cells of *P*1 KCs were cultured on 10-cm dish for 3 days and 1 week respectively. And then cells were treated with 50 µM AGR for 24 h. Cells were washed with PBS and collected from the dish by TrypLE select. Cells were lysed with 0.1% Triton X-100 and the macromolecules was removed using 10 kDa cut-off spin filter (Merck Millipore). The concentration of Ac-CoA in the cytolysis was measured using Coenzyme A Assay Kit (Sigma-Aldrich). The concentrations of Glucose and Lactate in the cytolysis were measured using Glucose Assay Kit-WST (Dojindo) and Lactate Assay Kit-WST (Dojindo). The component concentration in each sample was calculated from standard curve according to the manufacturer's procedure.

3. Results

3.1. Effect of AGR on cell viability

To investigate the effect of AGR (Fig. 1A) on cell viability, cells were treated with AGR at several concentrations for 24 h and their viability was measured using WST-8 assay (Fig. 1B).

The cell viability of human primary skin fibroblasts (NB1RGB), skin keratinocytes derived from human iPSCs (*P*1 KCs), and human colon cancer cells (HCT116) peaked at 0.05 µM (107%, 104%, and 102%). Above 0.5 µM, it decreased in a concentration-dependent manner, and the cell viability at 50 µM were 98%, 89%, and 96%, respectively. In contrast, AGR treatment drastically increased cell viability of iPSCs (*C*2 and 201B7) with the effect peaking at 50 µM (134% and 138%). We counted cell number after AGR treatment at indicated dose for 24 h. Cell number of AGR treated cells were normalized with no treated cells and shown as ratio in Fig. 1C. AGR increased cell proliferation in skin keratinocytes but not in fibroblasts and iPSCs. Cell cycle analysis by flow-cytometry in AGR treated skin keratinocytes showed increasing of G2/M population, confirming high proliferation rate (Fig. 1D). To examine whether AGR affect to the cell death, we used TUNEL assay. AGR treatment did not significantly affect to the cell death (Fig. 1 E). Moreover, AGR treated cells showed no significant change in ROS generation (Fig. 1F). Immunofluorescence with pluripotent marker OCT4 and SSEA4 antibodies showed AGR treatment did not affect to the pluripotency (Fig. 1G). These results suggested that the effect of AGR is dependent on the cell type and that AGR treatment increases cell viability in iPSCs.

3.2. Comprehensive gene expression analysis by RNA-seq in AGR-treated cells

Since AGR-induced cellular response differed depending on cell type, we compared gene expression changes by RNA-seq between NB1RGB fibroblasts, *C*2 iPSCs, and *P*1 KCs, which share the same genetic background. The number of upregulated genes (NB1RGB: 903, *C*2 iPSCs: 87, and *P*1 KCs: 205) and downregulated genes (NB1RGB: 634, *C*2 iPSCs: 42, and *P*1 KCs: 459) induced by AGR treatment with 50 µM for 4 h are shown in Fig. 2A.

Next, GO enrichment analysis was performed to investigate the association of AGR-upregulated genes. Fig. 2B shows the top 10 enriched terms of biological processes in each cell line. NB1RGB fibroblasts processes included increasing of cell cycle, cell division, DNA repair and *P*1 KCs processes included increasing of response to chemical and temperature stimuli; processes in *C*2 iPSCs included cellular developmental factors and organ morphogenesis. The $\log_2$ (fold change) of several genes upregulated were indicated by heat mapping (Fig. 2C). In NB1RGB fibroblasts, the expression of cell cycle regulatory genes increased, which have also been reported as IEGs in previous studies (Arner et al., 2015; Murai et al., 2020). In *C*2 iPSCs, the expression of IEGs such as *JUN* and *DUSP8* also increased. In addition, the expression of multiple genes related to development, e.g., *PAX5* and *ZIC1* for neural development (Adams et al., 1992; Aruga et al., 2011), *SP8* for limb development (Haro et al., 2014), and *INHBA* for testis development (Tomaszewski et al., 2007) was also affected. The expression of heat shock proteins (HSPs) and their co-chaperones was increased in *P*1 KCs. HSPs are protein-folding chaperones but are also related to keratinocyte differentiation, UVB protection, and DNA repair. The expression profile of HSPs has been reported to differ depending on the differentiation level of epidermal keratinocytes (Scieglinska et al., 2019). These results suggest that AGR-induced gene expression changes significantly differed among the three cell types, but were related to IEG response and differentiation.

3.3. Induction of IEGs by AGR

IEGs are usually induced very quickly within a few minutes following stimulation. Therefore, cells treated with AGR for 0.5–4 h were analyzed by RT-PCR (Fig. 3A and B). Expression of major IEGs, such as *JUN*, *FOS*, and *EGR1*, was increased in NB1RGB fibroblasts at a peak of 0.5–1 h. *EGR1* expression also peaked in 1 h in *C*2 iPSCs, but expression of *FOS* and *JUN* increased with treatment in a time-dependent manner. In contrast, expression of these genes did not increase in *P*1 KCs.

These results suggest that AGR induces typical IEG responses in NB1RGB fibroblasts, whereas those in iPSCs are different. Therefore, *C*2 iPSCs were treated with AGR for 4–24 h, and IEGs and differentiation-related factors were analyzed by RT-PCR (Fig. 4A and B). SRF, a major regulator of IEG expression, is essential for differentiation of PSCs into various cells (Connelly et al., 2010; Weinhold et al., 2000). In addition, CCND1 induced by JUN and FOS regulates PSCs differentiation (Pauklin et al., 2016; Pauklin et al.,2013). In *C*2 iPSCs, AGR treatment induced increases in expression of *SRF* and *CCND1,2,3* (cyclin Ds) along with that of the IEGs (*JUN*, *FOS*, *ATF3*, *DUSP6*, and *DUSP8*). The expression of *FOS*, *SRF*, *ATF*, and cyclin Ds in iPSCs *C*2 showed the same tendency in qRT-PCR (Supplemental Fig. 1). However, expression of *SRF* and cyclin Ds mRNA in NB1RGB fibroblasts was not significantly increased, indicating that this is a characteristic phenomenon of iPSCs.

3.4. Effect of AGR on cellular metabolism

High proliferation of PSCs depends on the energy efficiency of glycolysis. Since AGR treated iPSCs increased cell viability (Fig. 1B), we investigated effect of AGR on cellular metabolism. We found AGR treated iPSCs showed increasing of Ac-CoA, lactate, and glucose amount compared with no treated cells (Fig. 5). Furthermore, gene expression
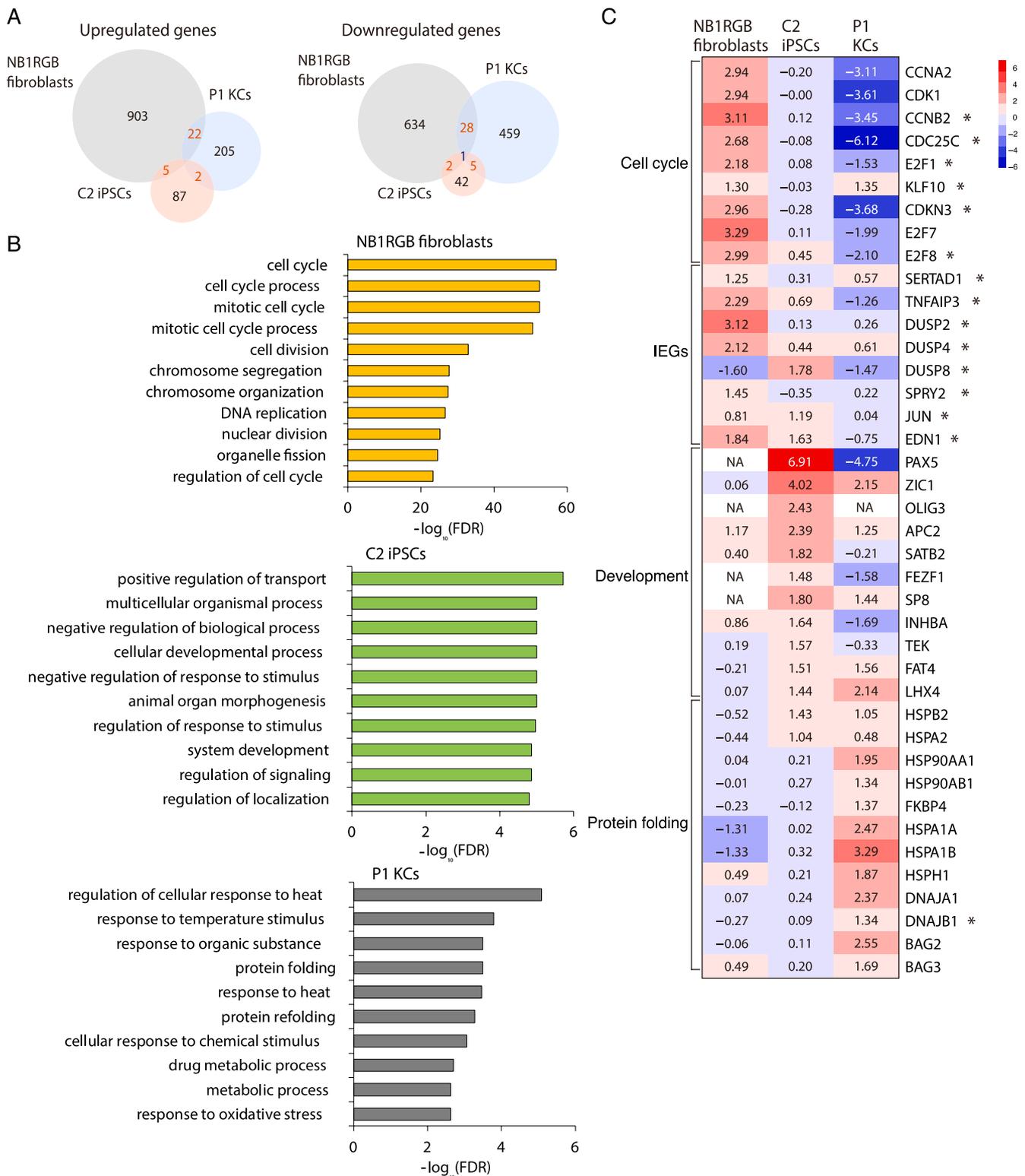
Fig. 2. Gene expression analysis by RNA sequencing in AGR treated cells.(A) Total RNA of AGR treated NB1RGB fibroblasts, C2 iPSCs, and P1 KCs was extracted and used for RNA sequencing analysis. Differential expression genes analysis was performed by DESeq2 and upregulated ($\log_2$ (fold change) > 1, P value < 0.01) or downregulated ($\log_2$ (fold change) < − 1, P value < 0.01) genes were shown. (B) Gene ontology analysis was performed by STRING. The top 10 biological process were plotted. (C) $\log_2$ (fold change) of genes upregulated by AGR in each cell was shown on heatmap. Genes reported as IEGs in previous studies (Arner et al., 2015; Murai et al., 2020) were marked with asterisk (*).

analysis revealed that AGR treatment transiently increased expression level of glycolysis and tricarboxylic acid (TCA) cycle pathway associated genes, pyruvate dehydrogenase (PDHB), ATP citrate synthase (ACLY), Ac-CoA synthetase (ACSS2), and uncoupling protein 2 (UCP2) genes in iPSCs. These results suggest that AGR transiently enhances cellular metabolism in PSCs.
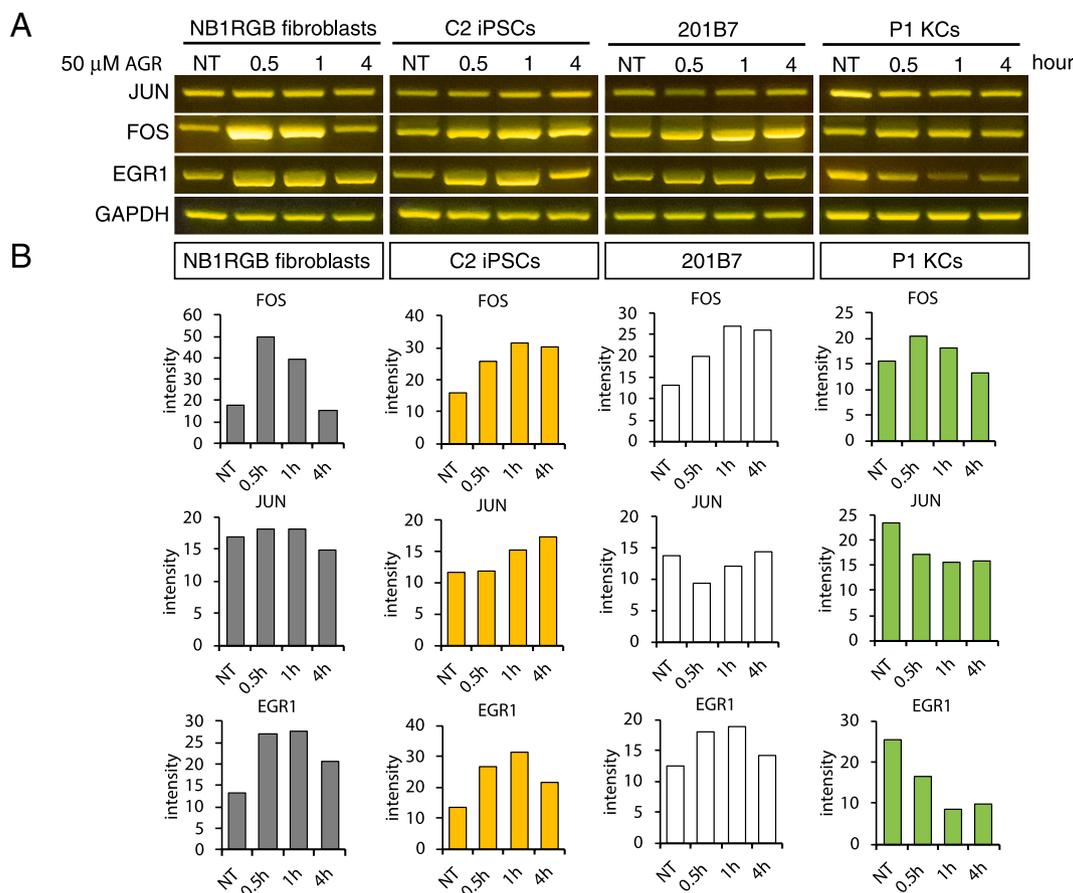
Fig. 3. IEGs expression analysis by RT-PCR in AGR treated cells.(A) Gene expression of IEGs, *JUN*, *FOS*, and *EGR1* assessed by RT-PCR in AGR-treated cells. *GAPDH* was used as loading control. (B) Intensities of PCR gel bands were measured by ImageJ software and graphed.
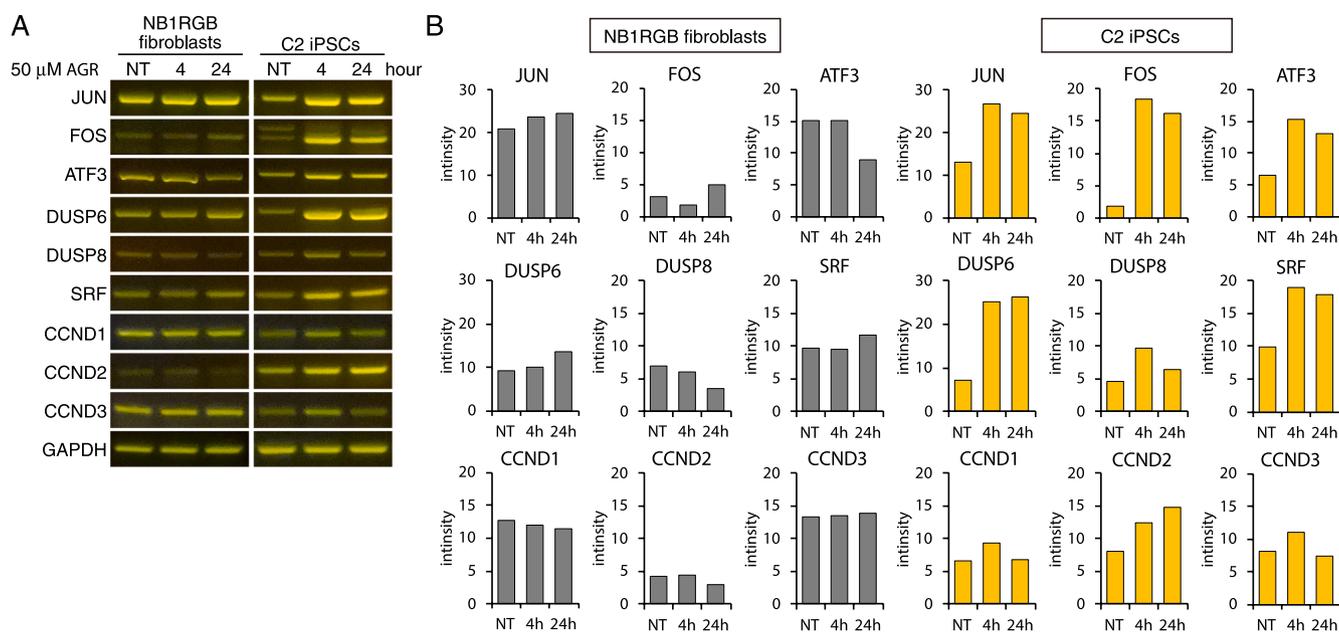

Fig. 4. IEGs and differentiation-related factors expression analysis by RT-PCR in AGR treated cells (A) Gene expression of IEGs (*JUN*, *FOS*, *ATF3*, *DUSP6*, and *DUSP8*) and differentiation-related factors (*SRF* and *CCND1,2,3*) were assessed by RT-PCR in AGR treated cells. *GAPDH* was used as loading control. (B) Intensities of PCR gel bands were measured by ImageJ software and graphed.

4. Discussion

We investigated the effect of AGR on gene expression, cell viability, cell cycle, and ROS generation between fibroblasts, iPSCs, and KCs differentiated from iPSCs. IEG expression was induced by AGR treatment in fibroblasts and iPSCs (Figs. 3 and 4), with a rapid and transient
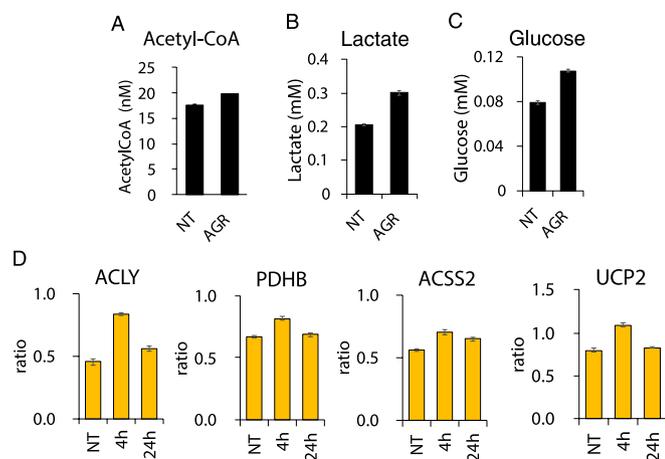
Fig. 5. AGR transiently enhances cell metabolism in iPSCs. (A-C) Concentration of intracellular metabolism-related components (A; Ac-CoA, B; Lactate, and C; Glucose,) at 50 μM AGR for 24 h was quantified. All experiments were independently performed three times. Error bar represented standard error. (D) Gene expression of metabolism-related factors (*ACLY*, *PDHB*, *ACSS2*, and *UCP2*) were assessed by qRT-PCR in AGR treated iPSCs.

response of IEG expression in NB1RGB fibroblasts. In contrast, the peak of IEG expression in iPSCs occurred after 4 h, which was delayed compared with that of the typical response. In previous studies, SLFN11-dependent IEG responses involved in chromatin remodeling also induced IEG expression in 4–6 h (Murai et al., 2020). AGR-induced IEG responses in iPSCs may also include chromatin remodeling.

In iPSCs, AGR treatment increased the expression of *SRF* and cyclin Ds mRNA along with IEG expression (Fig. 4). SRF is essential for IEG responses and differentiation in PSCs (Connelly et al., 2010; Schratt et al., 2001; Weinhold et al., 2000). Cyclin D1 is cell cycle regulator, and cell cycle regulation differs between PSCs and somatic cells (Liu et al., 2019). The short G1 phase of PSCs is related to pluripotency. With PSC differentiation, the G1 phase expands and the cyclin D1 expression increases accordingly. Cyclin D1 induces expression of genes that are involved in neuroectoderm differentiation along with cofactors such as P300 in the late G1 phase (Pauklin et al., 2016; Pauklin et al.,2013). Here, we observed upregulation of expression of neural development factors (*PAX5*, *ZIC1*, and *OLIG3*) in AGR treated iPSCs (Fig. 2). This suggests that differentiation signals to neuroectoderms were activated by AGR in iPSCs.

High proliferation and pluripotency of PSCs predominately contribute to glycolysis (Tsogtbaatar et al., 2020; Zhang et al., 2018). The energy efficiency of glycolysis is lower than that of oxidative phosphorylation (OxPhos), but the ATP synthesis speed is higher. Nucleotides and lipids can also be synthesized by glycolytic intermediates. Therefore, glycolysis can be adapted to rapid cell division and high proliferation in PSCs. Furthermore, reducing the level of ROS by OxPhos also helps maintain genomic stability. The Ac-CoA generated in glycolysis also maintains histone acetylation and pluripotency (Moussaieff et al., 2015). In the first 24 h of cell differentiation, glycolysis is reported to be turned off and coupled with OxPhos in PSCs, resulting in histone deacetylation and reduced levels of pluripotency markers. We showed that 24-h AGR treatment increased the cell viability of iPSCs, but not that of somatic cells (Fig. 1B). The WST8 assay used in this study measures cell viability by dehydrogenase activity. Therefore, if a change in dehydrogenase activity occurs this will affect correlation with cell viability. AGR treatment transiently increased gene expression of metabolic factors such as *ACLY, PDHB, ACSS2,* and *UCP2* (Fig. 5D). ACLY, PDHB, and ACSS2 are factors involved in the synthesis of Ac-CoA, and UCP2 plays a role in coupling glycolysis with OxPhos. It has been reported that UCP2 expression decreases with differentiation (Zhang et al., 2011). In addition, the concentration of intracellular metabolism-

related components, Ac-CoA, lactate, and glucose (Fig. 5A, B, and C), tended to increase with the AGR treatment, although pluripotency was maintained (Fig. 1G). Based on these results, we hypothesize that AGR transiently induces IEGs and metabolic factors at least for 4 h, and it gradually decreases resulting maintaining pluripotency.

In previous studies, we showed that *P*1 KCs has a faster DNA repair rate and higher radiosensitivity than more differentiated KCs (*P*2 and *P*3) (Miyake et al., 2019). We consider that *P*1 KCs are cycling precursors and also have properties similar to epidermal stem cells. In this study, the expression of HSPs related to keratinocyte differentiation was upregulated by AGR treatment in *P*1 KCs (Fig. 2); therefore, we expect that AGR promotes epidermal stem cell differentiation.

This study showed that AGR activates IEG-mediated differentiation signals and cellular metabolism in iPSCs. Thus, our results contribute to the elucidation of pluripotency and metabolic regulation in iPSCs.

5. Data statement

CRediT authorship contribution statement

Tomoko Miyake: Conceptualization, Methodology, Software, Data curation, Investigation, Writing - review & editing, Formal analysis, Writing - original draft, Visualization, Supervision, Project administration. **Munekazu Kuge:** Writing - review & editing. **Yoshihisa Matsumoto:** Writing - review & editing. **Mikio Shimada:** Conceptualization, Methodology, Writing - review & editing, Software, Formal analysis, Writing - original draft, Visualization, Data curation, Supervision, Project administration.

Declaration of Competing Interest

The authors declare the following financial interests/personal relationships which may be considered as potential competing interests: Tomoko Miyake reports financial support was provided by Takara Belmont Corp. Munekazu Kuge reports financial support was provided by Takara Belmont Corp. Mikio Shimada reports a relationship with Kato Memorial Bioscience Foundation that includes: funding grants. Mikio Shimada reports a relationship with Japan Atomic Energy Agency that includes: funding grants. Yoshihisa Matsumoto reports a relationship with Japan Society for the Promotion of Science that includes: funding grants. Tomoko Miyake has patent #2020-199611 pending to Munekazu Kuge, Hiroki Aoike, Tomoko Miyake. Munekazu Kuge has patent #2020-199611 pending to Munekazu Kuge, Hiroki Aoike, Tomoko Miyake. This work was funded by Takara Belmont Corp. Funder was not involved in study design, experiment, data analysis, manuscript preparation, or publication decisions. Among the authors, TM and MK are employed by Takara Belmont Corp. Our purpose is not to obtain direct financial benefits from this patent or paper.

Acknowledgements

Appendix A. Supplementary data

Supplementary data to this article can be found online at https://doi.org/10.1016/j.scr.2021.102511.

References

Adams, B., et al., 1992. Pax-5 encodes the transcription factor BSAP and is expressed in B lymphocytes, the developing CNS, and adult testis. Genes Dev. 6 (9), 1589–1607.

Aizawa, Y., et al., 2018. Design and evaluation of a novel flavonoid-based radioprotective agent utilizing monoglucosyl rutin. J. Radiat. Res. 59, 272–281.

Arner, E., et al., 2015. Transcribed enhancers lead waves of coordinated transcription in transitioning mammalian cells. Science 347, 1010–1015.

Aruga, J., et al., 2011. Role of BMP, FGF, calcium signaling, and zic proteins in vertebrate neuroectodermal differentiation. Neurochem. Res. 36 (7), 1286–1292.

Bahrami, S., et al., 2016. Gene regulation in the immediate-early response process. Adv. Biol. Regul. 62, 37–49.

Bejjani, F., et al., 2019. The AP-1 transcriptional complex: Local switch or remote command? Biochim. Biophys. Acta - Rev. Cancer 1872 (1), 11–23.

Connelly, J.T., et al., 2010. Actin and serum response factor transduce physical cues from the microenvironment to regulate epidermal stem cell fate decisions. Nat. Cell Biol. 12 (7), 711–718.

Engen, A., et al., 2015. Induction of cytotoxic and genotoxic responses by natural and novel quercetin glycosides. Mutat. Res. 784-785, 15–22.

Ganeshpurkar, A., Saluja, A.K., 2017. The Pharmacological Potential of Rutin. Saudi Pharm. J. 25 (2), 149–164.

Gualdrini, F., et al., 2016. SRF Co-factors Control the Balance between Cell Proliferation and Contractility. Mol. Cell 64 (6), 1048–1061.

Haro, E., et al., 2014. Sp6 and Sp8 Transcription Factors Control AER Formation and Dorsal-Ventral Patterning in Limb Development. PLoS Genet. 10 (8), e1004468.

Langfermann, D.S., et al., 2018. Stimulation of B-Raf increases c-Jun and c-Fos expression and upregulates AP-1-regulated gene transcription in insulinoma cells. Mol. Cell. Endocrinol. 472, 126–139.

Liu, L., et al., 2019. The cell cycle in stem cell proliferation, pluripotency and differentiation. Nat. Cell Biol. 21 (9), 1060–1067.

Miyake, T., et al., 2019. DNA Damage Response After Ionizing Radiation Exposure in Skin Keratinocytes Derived from Human-Induced Pluripotent Stem Cells. Int. J. Radiat. Oncol. Biol. Phys. 105 (1), 193–205.

Moussaieff, A., et al., 2015. Glycolysis-mediated changes in acetyl-CoA and histone acetylation control the early differentiation of embryonic stem cells. Cell Metab. 21 (3), 392–402.

Murai, J., et al., 2020. Chromatin Remodeling and Immediate Early Gene Activation by SLFN11 in Response to Replication Stress. Cell Rep. 30 (12), 4137–4151.e6.

Nihashi, Y., et al., 2019. Distinct cell proliferation, myogenic differentiation, and gene expression in skeletal muscle myoblasts of layer and broiler chickens. Sci. Rep. 9 (1), 16527.

Pauklin, S., et al., 2016. Initiation of stem cell differentiation involves cell cycle-dependent regulation of developmental genes by Cyclin D. Genes Dev. 30 (4), 421–433.

Pauklin, S., et al., 2013. The cell-cycle state of stem cells determines cell fate propensity. Cell 155 (1), 135–147.

Prasad, R., et al., 2019. A review on the chemistry and biological properties of Rutin, a promising nutraceutical agent. Asian J. Pharm. Pharmacol. 5 (S1), 1–20.

Schratt, G., et al., 2001. Serum Response Factor Is Required for Immediate-Early Gene Activation yet Is Dispensable for Proliferation of Embryonic Stem Cells. Mol. Cell. Biol. 21 (8), 2933–2943.

Scieglinska, D., et al., 2019. Heat shock proteins in the physiology and pathophysiology of epidermal keratinocytes. Cell Stress Chaperones 24, 1027–1044.

Shaulian, E., et al., 2002. AP-1 as a regulator of cell life and death. Nat. Cell Biol. 4 (5), E131–E136.

Shimada, M., et al., 2019. Reprogramming and differentiation-dependent transcriptional alteration of DNA damage response and apoptosis genes in human induced pluripotent stem cells. J. Radiat. Res. 60, 719–728.

Shimoi, K., et al., 2003. Absorption and urinary excretion of quercetin, rutin, and αG-rutin, a water soluble flavonoid, in rats. J. Agric. Food Chem. 51 (9), 2785–2789.

Suzuki, Y., et al., 1991. Enzymatic formation of 4G-α-D-glucopyranosyl-rutin. Agric. Biol. Chem. 55, 181.

Szklarczyk, D., et al., 2017. The STRING database in 2017: Quality-controlled protein-protein association networks, made broadly accessible. Nucleic Acids Res. 45 (D1), D362–D368.

Tomaszewski, J., et al., 2007. Essential roles of inhibin beta A in mouse epididymal coiling. Proc. Natl. Acad. Sci. U.S.A. 104 (27), 11322–11327.

Tsogtbaatar, E., et al., 2020. Energy Metabolism Regulates Stem Cell Pluripotency. Front. Cell Dev. Biol. 8 https://doi.org/10.3389/fcell.2020.00087.

Vitale, I., et al., 2017. DNA Damage in Stem Cells. Mol. Cell. 66 (3), 306–319.

Weinhold, B., et al., 2000. Srf(-/-) ES cells display non-cell-autonomous impairment in mesodermal differentiation. EMBO J. 19, 5835–5844.

Zhang, J., et al., 2018. Metabolism in Pluripotent Stem Cells and Early Mammalian Development. Cell Metab. 27 (2), 332–338.

Zhang, J., et al., 2011. UCP2 regulates energy metabolism and differentiation potential of human pluripotent stem cells. EMBO J. 30, 4860–4873.